

Modeling spatially explicit fire impact on gross primary production in interior Alaska using satellite images coupled with eddy covariance

Shengli Huang ^{a,1}, Heping Liu ^b, Devendra Dahal ^c, Suming Jin ^{a,1}, Lisa R. Welp ^d,
Jinxun Liu ^{c,2}, Shuguang Liu ^{e,*}

^a ASRC Research and Technology Solutions (ARTS), Contractor to the U.S. Geological Survey (USGS) Earth Resources Observation and Science (EROS) Center, 47914 252nd Street, Sioux Falls, SD 57198, USA

^b Department of Civil and Environmental Engineering, Washington State University, Pullman, WA 99164, USA

^c Stinger Ghaffarian Technologies (SGT), Inc., Contractor to the USGS EROS Center, Sioux Falls, SD 57198, USA

^d Scripps Institution of Oceanography, University of California, San Diego, La Jolla, CA 92093-0244, USA

^e USGS EROS Center, 47914 252nd Street, Sioux Falls, SD 57198, USA

ARTICLE INFO

Article history:

Received 16 November 2012
Received in revised form 5 April 2013
Accepted 6 April 2013
Available online 3 May 2013

Keywords:

Remote sensing
Image reconstruction
Eddy covariance
Vegetation production
Gross primary production
Fire
Alaska

ABSTRACT

In interior Alaska, wildfires change gross primary production (GPP) after the initial disturbance. The impact of fires on GPP is spatially heterogeneous, which is difficult to evaluate by limited point-based comparisons or is insufficient to assess by satellite vegetation index. The direct prefire and postfire comparison is widely used, but the recovery identification may become biased due to interannual climate variability. The objective of this study is to propose a method to quantify the spatially explicit GPP change caused by fires and succession. We collected three Landsat images acquired on 13 July 2004, 5 August 2004, and 6 September 2004 to examine the GPP recovery of burned area from 1987 to 2004. A prefire Landsat image acquired in 1986 was used to reconstruct satellite images assuming that the fires of 1987–2004 had not occurred. We used a light-use efficiency model to estimate the GPP. This model was driven by maximum light-use efficiency (E_{\max}) and fraction of photosynthetically active radiation absorbed by vegetation (F_{PAR}). We applied this model to two scenarios (i.e., an actual postfire scenario and an assuming-no-fire scenario), where the changes in E_{\max} and F_{PAR} were taken into account. The changes in E_{\max} were represented by the change in land cover of evergreen needleleaf forest, deciduous broadleaf forest, and shrub/grass mixed, whose E_{\max} was determined from three fire chronosequence flux towers as 1.1556, 1.3336, and 0.5098 gC/MJ PAR. The changes in F_{PAR} were inferred from NDVI change between the actual postfire NDVI and the reconstructed NDVI. After GPP quantification for July, August, and September 2004, we calculated the difference between the two scenarios in absolute and percent GPP changes. Our results showed rapid recovery of GPP post-fire with a 24% recovery immediately after burning and 43% one year later. For the fire scars with an age range of 2–17 years, the recovery rate ranged from 54% to 95%. In addition to the averaging, our approach further revealed the spatial heterogeneity of fire impact on GPP, allowing one to examine the spatially explicit GPP change caused by fires.

Published by Elsevier Inc.

1. Introduction

Gross primary production (GPP) is the amount of carbon fixed by vegetation through photosynthetic assimilation; it is critical in land surface–atmosphere interactions and a key component of ecosystem carbon fluxes and the carbon balance between the biosphere and the atmosphere (Mäkelä et al., 2008). The quantification of carbon fluxes between the terrestrial biosphere and the atmosphere is of scientific importance and relevant to climate policy making (Xiao et al., 2010). In a boreal region, the vegetation production plays an

important role in the global cycles of carbon and the climate system (Melillo et al., 1993; Schulze et al., 1999). However, fire is the primary disturbance agent in most of the North American boreal forest; the frequency of large fires has increased dramatically over the past four decades and fire frequency and severity may increase further due to climate warming (Kasischke and Turetsky, 2006; Kasischke et al., 2011; Yi et al., 2010). After a disturbance, carbon dynamics are primarily driven by GPP (Amiro et al., 2010; Goulden et al., 2011).

The successional trajectories of boreal forests after fires are various (Beck et al., 2011; Johnstone et al., 2010; Shenoy et al., 2011). More frequent and larger fires in the late twentieth century resulted in deciduous trees and mosses increasing production at the expense of coniferous trees (Bond-Lamberty et al., 2007). Consequently, wildfires strongly influence boreal forest age structure, species composition, and thus vegetation photosynthesis process, affecting the carbon cycle and climate,

* Corresponding author. Tel.: +1 605 5946168.

E-mail address: sliu@usgs.gov (S. Liu).

¹ Work performed under USGS contract G08PC91508.

² Work performed under USGS contract G10PC00044.

which may persist for many decades (Bond-Lamberty et al., 2004; Randerson et al., 2006). This illustrates the need for a comprehensive examination of the magnitude and direction of changes in primary productivity as a result of altered ecosystem processes (Beck and Goetz, 2011).

Eddy covariance flux towers, which directly measure net ecosystem exchange (NEE) separable into GPP and ecosystem respiration (Re) (Baldocchi et al., 2001; Reichstein et al., 2005), and field measurements can be used to study the fire impact on carbon fixation. For example, Bond-Lamberty et al. (2004), Litvak et al. (2003), Goulden et al. (2006), Welp et al. (2006), and Goulden et al. (2011) all investigated carbon dynamics for chronosequence of postfire boreal forest stands based on field or flux measurements. These site-specific field measurement and flux observation studies have provided excellent information and aided a better understanding of the vegetation production associated with fire. Unfortunately, the high spatial and temporal variability of terrestrial ecosystems across complex landscapes results in a challenging task of regional extrapolation from point-based GPP measurements (Maselli et al., 2009). Significant efforts are still needed to upscale field observations or flux tower measurements from the stand scale to landscape, regional, continental, or global scales to advance toward explicitly incorporating the impacts of disturbance on ecosystem carbon exchange (Xiao et al., 2010, 2012), because the long-term carbon effects of fire disturbance are spatially heterogeneous at scales of 10 m to approximately 1000 m due to the complex interactions and the variation of burn severity, topography, drainage, prefire vegetation condition, and weather (Goetz et al., 2012; Huang et al., 2013).

Due to the weakness of spatial representation of point-based study, consistent and spatially continuous satellite remote sensing has played an increasing role in production estimation (Goetz et al., 1999; Potter et al., 1993). Several studies used satellite vegetation index to examine forest recovery in the boreal region. Kasischke and French (1997) analyzed Normalized Difference Vegetation Index (NDVI) of 14 test sites in the boreal forest of interior Alaska to examine the patterns of recovery. Epting and Verbyla (2005) used Landsat vegetation index to analyze the vegetation recovery. Goetz et al. (2006) compared NDVI anomalies of burned and unburned areas to analyze fire disturbance and forest recovery across Canada. Cuevas-González et al. (2009) used satellite vegetation index to analyze forest recovery after wildfire disturbance in boreal Siberia. Veraverbeke et al. (2012) assessed postfire vegetation recovery using red–near infrared vegetation indices. Unitless vegetation index is a good proxy of vegetation production, but it does not reflect the GPP quantity in a unit such as $\text{gC/m}^2/\text{month}$. However, it can be coupled with a vegetation production model such as light-use efficiency model for this purpose. Amiro et al. (2000) modeled NPP from the Advanced Very High Resolution Radiometer (AVHRR) leaf area index (LAI) and assessed forest carbon budgets following fire across Canada at the ecoregion level. Hicke et al. (2003) assessed the impact of 61 large fires on prefire and postfire NPP in the North American boreal forest using a 17-year record of satellite NDVI observations coupled with a carbon model. Since the interannual climate variability such as drought can influence successional vegetation production (Welp et al., 2007), an approach that examines fire-induced spatially explicit carbon fixation by minimizing the influence of other confounding factors (e.g., weather, soil, phenology) is still desired.

The objective of this study is to demonstrate a method of using eddy flux measurements, satellite images, and models to examine the spatially explicit impact of fire on vegetation production. Satellite images have been coupled with eddy covariance measurements to scale point-based fluxes to regional GPP (Ueyama et al., 2010; Wang et al., 2010a; Xiao et al., 2010). Based on the knowledge gained from these previous studies, we aim to further understand the relationship between disturbances and ecosystem dynamics. To achieve this goal, we used eddy covariance towers, which are located at two burned sites and one unburned site, to parameterize a vegetation photosynthesis model. This model estimated GPP from a satellite vegetation index and climate based on a light-use efficiency concept. This model was applied to two scenarios. In one

scenario, actual postfire satellite images were used to drive the GPP model, and in the other scenario, reconstructed satellite images, where no fire was assumed to have occurred, were used to drive the GPP model. By comparing the pixel-by-pixel difference, the spatially explicit impact of fire on GPP was revealed.

2. Study area

Our study covered an area of 110 km by 130 km in the interior of Alaska and was conducted near Delta Junction, which is centered at 145.535 W and 64.293 N and covers a 110 km \times 130 km area (Fig. 1). Based on the climate record at Big Delta (64.000 N, 145.440 W), Welp et al. (2006) reported that the average daily minimum temperature in January was -24°C and the average daily maximum during July was 21°C . The growing season length was approximately 115 days from mid-May to early September. The elevation ranges from 213 m to 1872 m, with a mean of 590 m and standard deviation of 262 m. National Land Cover Database 2001 (NLCD 2001, <http://www.mrlc.gov/>) data indicate that the vegetation cover is dominated by deciduous broadleaf forest (17%), evergreen needleleaf forest (46%), and shrub/scrub (20%). Based on the permafrost map (<http://agdcwww.wr.usgs.gov/agdc/agdc.html>), the area features a “mountainous area underlain by discontinuous permafrost” (77.73%), a “lowland and upland area underlain by numerous isolated masses of permafrost” (21.89%), and a “lowland and upland area underlain by moderately thick to thin permafrost” (0.38%).

Within this study area, we set up three sites for field survey: one that burned in 1987, one that burned in 1999, and one that burned in approximately 1920. These sites were located on relatively well drained silty loam soil and will be hereinafter referred to as the 1987 burn, 1999 burn, and control sites (Fig. 1). In the 1999 burn site, the Donnelly Flats crown fire consumed much of the aboveground biomass and soil organic matter. In 2002, there were 2691 ± 778 standing dead boles of black spruce per hectare with a mean height of 4 m, and 30% of the ground surface was covered by bunch grasses (*Festuca altaica*) and deciduous shrubs less than 1 m tall. In the 1987 burn site, the Granite Creek fire killed all of the aboveground vegetation, primarily black spruce. By 2002, some of the dead spruce boles remained standing, but most had fallen over. In 2002, the stand was dominated by an overstory of willow shrubs (*Salix* spp.) and deciduous aspen trees (*Populus tremuloides*) with a mean canopy height of 5 m and a density of 3956 ± 370 trees per hectare. The sparse understorey vegetation included shrubs (*Salix* spp., *Ledum palustre*, *Rosa acicularis*, *Vaccinium uliginosum*, and *Vaccinium vitis-idaea*), black spruce (*Picea mariana*), and grasses (*Festuca* spp. and *Calamagrostis lapponica*) separated by patches of moss in open areas (*Polytrichum* spp.). In the control site, the canopy overstorey consisted of homogeneous stands of black spruce (*P. mariana*) with a mean canopy height of 4 m and a mean age of 80 years. The mean canopy height was 4 m, and the sparse understorey consisted of shrubs (*L. palustre*, *V. uliginosum* and *V. vitis-idaea*). The dominant ground cover was feathermoss (*Pleurozium schreberi* and *Rhytidium rugosum*) and lichen (*Cladonia* spp. and *Stereocaulon* spp.).

3. Dataset

3.1. Eddy covariance

CO_2 fluxes of three stands that were part of a fire chronosequence in interior Alaska (i.e., 1999 burn, 1987 burn, and control sites) were measured using the eddy covariance method (Fig. 1). From 2002 to 2004, eddy covariance measurements of NEE CO_2 fluxes were made at each stand and averaged at 30-min intervals along with vertical and horizontal wind velocity, sonic temperature, concentrations of CO_2 and water vapor, above-canopy incoming shortwave radiation and photosynthetic photon flux density (PPFD), precipitation, and vapor pressure deficit (VPD). Soil moisture and temperature at 10 cm

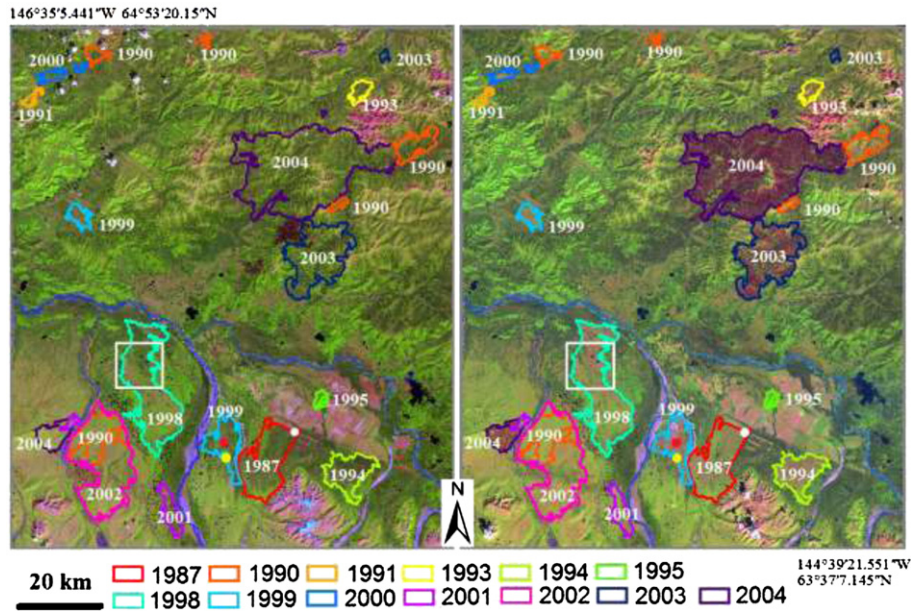


Fig. 1. Study area. The fires that occurred during 1987–2004 are overlaid with the 26 June 1986 (left) and 5 August 2004 (right) Landsat R5G4B3 composites, where evergreen needleleaf forest is shown as dark green, deciduous broadleaf forest as bright green, and shrub/grass mixed as light green or reddish. Gross primary production was extracted from three towers located at a 1987 burn (white dot), a 1999 burn (red dot), and an unburned control site (yellow dot) (see Section 4.3). For visual purpose, the dots of the towers were exaggerated, but their exact coordinates can be found in Liu and Randerson (2008). Spatial variation of the land surface was examined in a 10.5 km × 11.5 km area (white rectangle, see Section 5).

depth were also recorded. Instrument configuration was reported by Liu et al. (2005).

3.2. Satellite images, climate, DEM, and fires

Four Landsat scenes from 26 June 1986 (path 67 row 15), 13 July 2004 (path 67 row 15), 5 August 2004 (path 68 row 15), and 6 September 2004 (path 68 row 15) at 30 m resolution were collected. We focused on the fires that occurred during 1987 and 2004; therefore, a prefire Landsat image of 1986 was selected. After very few clouds and shadows were excluded with the method of Jin et al. (2012), the raw digital numbers of Landsat were converted to radiance and reflectance (Huang et al., 2013). A Digital Elevation Model (DEM) at 60 m resolution was

collected from the USGS National Elevation Dataset. Monthly average temperature and total precipitation at 771 m resolution were download from “Scenarios Network for Alaska and Arctic Planning” of University of Alaska (SNAP, <http://www.snap.uaf.edu/>). Fire polygons and burn severity derived from Landsat images were downloaded from the Monitoring Trends in Burn Severity (MTBS, <http://mtbs.gov>).

4. Method

4.1. Overview

Many satellite-based studies have used the light-use efficiency approach to estimate either GPP or NPP (e.g., Field et al., 1995;

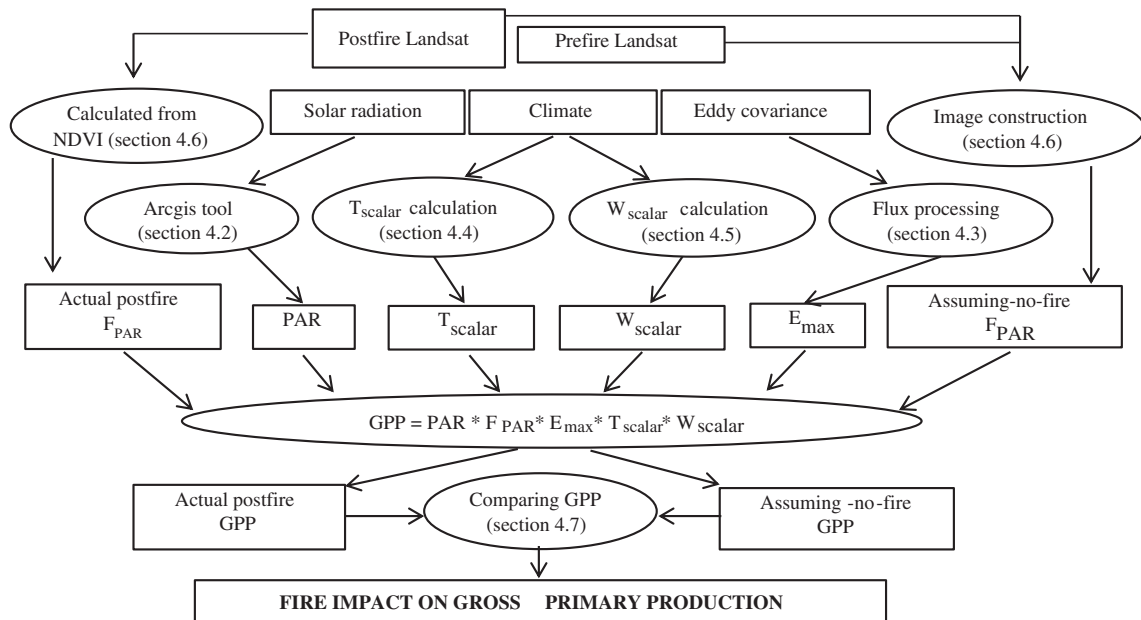


Fig. 2. Flowchart of modeling fire impact on gross primary production.

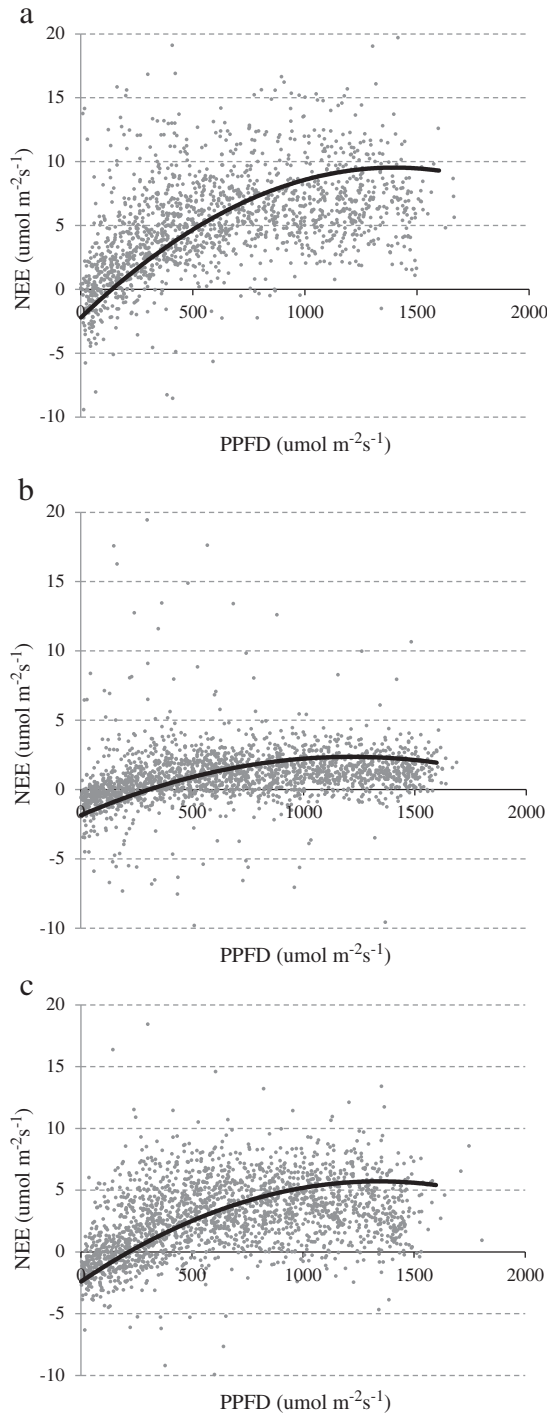


Fig. 3. The relationship between net ecosystem exchange-photosynthetic photon flux density (NEE–PPFD) as measured by the eddy covariance flux towers for a) 1987 burn, b) 1999 burn, and c) unburned control sites. The positive NEE values are uptake by the ecosystem.

Landsberg and Waring, 1997; Li et al., 2007; Potter et al., 1993; Prince and Goward, 1995; Ruimy et al., 1996; Running et al., 2000; Xiao et al., 2004a, b). We also used a light-use efficiency model to assess the fire impact on GPP (Eq. 1):

$$\text{GPP} = \text{PAR} * F_{\text{PAR}} * E_{\text{max}} * T_{\text{scalar}} * W_{\text{scalar}} \quad (1)$$

where PAR is the monthly incident photosynthetically active radiation (MJ m^{-2} , see Section 4.2), E_{max} is the apparent quantum yield or maximum light-use efficiency (gC/MJ PAR , see Section 4.3), and

T_{scalar} (see Section 4.4) and W_{scalar} (see Section 4.5) are the downward regulation scalars for the effects of temperature and water on light-use efficiency of vegetation, respectively. F_{PAR} is the fraction of PAR absorbed by vegetation canopy. In our study, we calculated the actual postfire F_{PAR} , but we also used an image reconstruction approach to model the F_{PAR} assuming the fires had not occurred (see Section 4.6). The comparison between these two scenarios enabled us to quantify the GPP change caused by fires and succession (see Section 4.7). Fig. 2 depicts the general flowchart.

4.2. PAR

PAR designates the spectral range of solar radiation from 400 to 700 nm that photosynthetic organisms are able to use in the process of photosynthesis. In this study, monthly PAR was calculated as 0.48 of monthly incoming shortwave radiation (INSOLAR), where 0.48 is the ratio of PAR to INSOLAR (McCree, 1972). INSOLAR received during July, August, and September 2004 was calculated from the ArcGIS solar radiation tool. This tool accounts for the effect of atmospheric conditions, site latitude, elevation, slope, aspect, sun angle, and shadows cast by surrounding topography on the amount of INSOLAR. It requires the user input of a spatially explicit DEM as well as transmittivity and diffuse proportion (Huang et al., 2008). The transmittivity and diffuse proportion were calibrated for each month so that the INSOLAR were approximate to measured values from flux towers.

4.3. E_{max} of fire chronosequence

Because the land surface changed after a fire disturbance, we classified vegetation from two Landsat Thematic Mapper (TM) scenes, prefire June 1986 and postfire August 2004, using the unsupervised Self-Organization Data Analysis Techniques Algorithm (ISODATA, Mather, 1987). Spectral classes were grouped into three vegetation types: evergreen needleleaf forest, deciduous broadleaf forest, and shrub/grass mixed. Different vegetation types have different E_{max} values, but E_{max} can be inferred from eddy flux towers based on NEE of CO_2 and PPFD (Goulden et al., 1997). We estimated E_{max} from the three flux towers of the 1987 burn, 1999 burn, and the unburned control sites, which represent the local typical ecosystem types of deciduous broadleaf forest, shrub/grass mixed, and evergreen needleleaf forest, respectively. This was achieved through two steps: 1) gap-filling missed measurements and partitioning NEE into GPP and R_e , and 2) fitting the Michaelis–Menten function to estimate E_{max} , as described below.

Data quality control of eddy covariance and meteorological measurements was implemented, gaps in the observations were filled, and half-hourly NEE fluxes were partitioned into R_e and GPP. The detailed approach was described by Welp et al. (2006, 2007). Briefly, missing R_e was estimated from a temperature-dependent Q10 respiration model that was mathematically equivalent to a Van't Hoff exponential model (Lloyd and Taylor, 1994). During daytime periods of missing NEE observations, GPP was modeled using a Michaelis–Menten model based on Zha et al. (2004) but with the effect of VPD taken into account. Monthly GPP for these three sites was calculated from the half-hourly observations.

There is a near-linear increase in productivity at low light levels and an asymptotic approach to maximum productivity at high light levels; therefore, a rectangular hyperbola function can be used to represent the relation between gross productivity and incident PAR (Frolking et al., 1998). Based on the daytime data within the peak growing season from July 1 to July 31 in 2002–2004, we estimated the nonlinear model between NEE and PAR by fitting the rectangular hyperbolic Michaelis–Menten function (Eq. 2 and Fig. 3) to obtain the E_{max} values of the 1987 burn, 1999 burn, and control sites.

$$\text{NEE} = \frac{E_{\text{max}} \times \text{PPFD} \times P_{\text{max}}}{E_{\text{max}} \times \text{PPFD} \times P_{\text{max}} + R_e} \quad (2)$$

Table 1
Parameters of Michaelis–Menten in three sites.

Sites	n	E_{\max}^a		P_{\max}^b		R^2	F-test
		$\mu\text{mol CO}_2/\mu\text{mol PPFD}$	gC/mol PAR	gC/MJ PAR	$\mu\text{mol CO}_2 \text{ m}^{-2} \text{ s}^{-1}$		
1999 burn	1986	0.0092	0.1104	0.5098	4.9378	0.281	$P < 0.001$
1987 burn	1614	0.0242	0.2904	1.3336	19.9304	0.545	$P < 0.001$
Control	2048	0.0209	0.2508	1.1556	11.7168	0.448	$P < 0.001$

^a Maximum light-use efficiency in different units based on an approximate conversion of 4.6 between MJ (10^6 J) and mol PPFD (McCree, 1981) and of 12.001 between mol CO_2 and gC.

^b P_{\max} is the maximum gross ecosystem exchange.

where PPFD is the photosynthetic photon flux density of PAR, E_{\max} is the maximum light-use efficiency or apparent quantum yield (as PPFD approaches to 0), P_{\max} is the maximum gross ecosystem exchange, and R_e is the ecosystem respiration. The E_{\max} values are summarized in Table 1.

4.4. T_{scalar}

T_{scalar} is estimated at each month at each grid, using Eq. (3) developed for the CASA model (Potter et al., 1993).

$$T_{\text{scalar}} = \frac{1.1814 * (0.8 + 0.02T_{\text{opt}} - 0.0005T_{\text{opt}}^2) * (1 + \exp[0.3 * (T - 10 - T_{\text{opt}})])}{1 + \exp[0.2 * (T_{\text{opt}} - 10 - T)]} \quad (3)$$

where T_{opt} is the optimal temperature defined as the monthly mean temperature in July when vegetation has the maximum canopy. If T is lower than 0°C , T_s is set as 0; if T_s is greater than 1, T_s is set as 1 (Potter et al., 1993).

4.5. W_{scalar}

The effect of water on plant photosynthesis (W_{scalar}) was estimated based on the atmospheric water supply–demand concept. Monthly moisture effects based on the “supply–demand” drought index (SDDI) approach (Rind et al., 1990) were used. For a month of interest i , its potential evapotranspiration (PET) was first calculated using Hamon method (Eq. 4, Lu et al., 2005):

$$\text{PET}_i = 0.1651 * 216.7 * (d/12) * (6.108 * e^{(17.27T/(T+237.3))} / (T + 273.3)) \quad (4)$$

where d is the total daylength in hours and T is the average monthly temperature ($^\circ\text{C}$). Second, for each grid we calculated an index Z_i :

$$Z_i = [(PPT_i - \text{PET}_i) - (PPT_i^* - \text{PET}_i^*)] / \text{STD}_i \quad (5)$$

where PPT_i is the precipitation, PPT_i^* is the long-term average precipitation, PET_i^* is the long-term average PET, STD_i is the interannual standard deviation of the $PPT - \text{PET}$ for month i . Third, to account for the fact that soil moisture deficit is a cumulative phenomenon, the index for the current month Y_i , which is related to the index from the previous month Y_{i-1} , was calculated following Rind et al. (1990):

$$Y_i = 0.897 Y_{(i-1)} + Z_i \quad (6)$$

Last, we converted Y_i to water stress scalar W_{scalar} :

$$W_{\text{scalar}} = 0.5 + 0.5 * [Y_i - Y_{i \text{ min}}] / [Y_{i \text{ max}} - Y_{i \text{ min}}] \quad (7)$$

where $Y_{i \text{ max}}$ and $Y_{i \text{ min}}$ are the maximum and minimum Y_i for month i .

4.6. F_{PAR} change between two scenarios

F_{PAR} depicts how much PAR can be absorbed by vegetation canopy. In our study, the “best” and “local” $F_{\text{PAR}} - \text{NDVI}$ relationship for all plant functional types was used to estimate F_{PAR} from Landsat NDVI (Eq. 8, Steinberg et al., 2006).

$$F_{\text{PAR}} = \text{MAX}\{0, \text{MIN}[(1.26 \text{ NDVI} + 0.011), 0.95]\} \quad (8)$$

where NDVI was calculated as a normalized ratio between the near-infrared band (B4) and the red band (B3) using Eq. (9) (Tucker, 1979), resulting in three NDVI datasets for 13 July, 5 August, and 6 September 2004.

$$\text{NDVI} = (B4 - B3) / (B4 + B3) \quad (9)$$

One main purpose of our study is to examine the fire impact on GPP at the pixel level; this requires NDVI datasets (and thus F_{PAR}) assuming the fires had not occurred. Huang et al. (2013) had developed an approach to reconstruct the land surface, including NDVI, assuming no fires had occurred (Fig. 4). Briefly, a prefire image was selected as a reference and spectral characteristics of the same location as the fire pixel were first derived from the reference scene; second, spectrally similar pixels were identified within the reference scene; third, pixels that were not burned in the target scene, but were spectrally similar to the fire pixel on the reference scene, were averaged to provide an estimate for the fire pixel. In our study, taking the 26 June 1986 Landsat scene as a reference, we used the same concept to reconstruct 1987–2004 fire scars for 13 July 2004, 5 August 2004, and 6 September 2004. The NDVI was calculated for the reconstructed images, resulting in three NDVI datasets for 13 July, 5 August, and 6 September 2004 for the assuming-no-fire scenario.

4.7. GPP comparison and fire impact analysis

GPP under two scenarios (i.e., actual postfire GPP and assuming-no-fire GPP) was calculated using Eq. (1). This calculation resulted

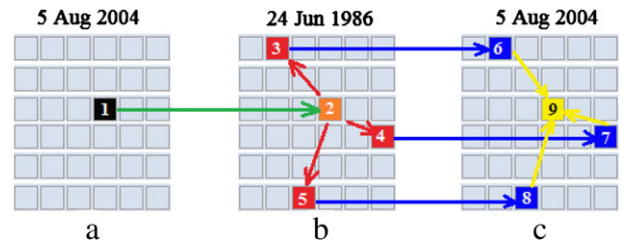


Fig. 4. Conceptual flowchart of reconstructing Landsat reflectance. For a burned pixel on 5 August 2004 (pixel 1 in a), its corresponding pixel was located on 26 June 1986 (pixel 2 in b). The pixels with similar reflectance were determined in 26 June 1986 (pixels 3, 4, and 5 in b). The locations of these pixels were then reprojected back to 5 August 2004 (pixels 6, 7, and 8 in c). The mean value of these pixels was the reconstructed reflectance for the impacted pixel (pixel 9 in c).

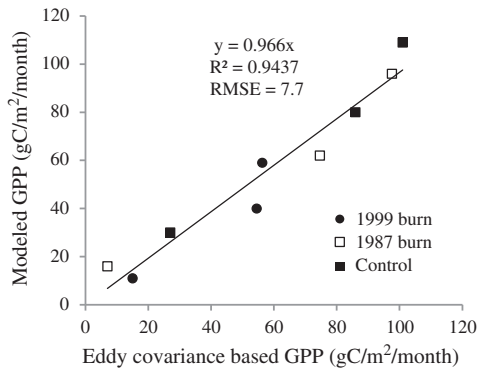


Fig. 5. Comparison of monthly modeled and eddy covariance based GPP for July, August, and September 2004 within the footprint size of 8100 m².

in six GPP datasets, three for 13 July, 5 August, and 6 September 2004 under the actual postfire scenario and the other corresponding three under the assuming-no-fire scenario. The GPP difference between these two scenarios resulted from the change in E_{\max} and F_{PAR} as follows.

- 1) E_{\max} : Different vegetation has a different E_{\max} value (Table 1). For example, for one pixel, the prefire vegetation type in 1986 was evergreen needleleaf forest, but it changed to deciduous broadleaf forest in 2004. Accordingly, the E_{\max} of 1.1556 gC/MJ PAR and 1.3336 gC/MJ PAR was used for the assuming-no-fire and actual postfire scenarios, respectively.
- 2) F_{PAR} : Different vegetation has different NDVI (and thus F_{PAR}). Taking the same example above, the assuming-no-fire NDVI was 0.4 and the actual postfire NDVI was 0.7. According to Eq. (8), the F_{PAR} of 0.515 and 0.893 was used for the assuming-no-fire and actual postfire scenarios, respectively.

At each flux tower location, the mean modeled GPP was compared with GPP based on eddy covariance. Since we have 3 flux towers (1987 burn, 1999 burn, and control sites) and 3 months (July, August, and September 2004), we compared 9 GPP pair values. This comparison helped to evaluate the reliability of our GPP modeling.

Fire impact on GPP was quantified by subtracting actual postfire GPP and assuming-no-fire GPP, aiding us in examining the absolute GPP magnitude change. However, due to cloud cover, only July, August, and September 2004 images were used, which resulted in incomplete GPP analysis of a full growing season. In addition, the 2004 drought resulted in lower GPP than normal years (Welp et al., 2007). A relative recovery rate, which is the ratio of the actual postfire GPP to assuming-no-fire GPP, would reduce the influence

of GPP fluctuation caused by interannual climate variability and was thus further examined to aid the analysis.

5. Result

The modeled and eddy covariance based GPP for July, August, and September 2004 is plotted in Fig. 5. The modeled GPP agreed with eddy covariance based GPP well with an R^2 of 0.9437 and a root mean square error (RMSE) of 7.7 gC/m²/month, indicating the reliability of our GPP modeling.

With the GPP model applied to two scenarios, the spatial distribution of GPP of the actual postfire and assuming-no-fire scenarios and their difference is shown in Fig. 6, where the general spatial GPP pattern affected by fire disturbance is clearly visible. The lower left corner (fire scars of 1990 and 2002) has very close or even slightly higher actual postfire GPP than assuming-no-fire GPP, indicating almost complete recovery. The prefire vegetation of this area was shrub/grass mixed, the same as postfire vegetation. The upper right corner (fire scars of 2003 and 2004) shows the lowest negative GPP difference, indicating less GPP recovery during the earliest succession stage. The prefire vegetation of this area was evergreen needleleaf forest, different from the postfire vegetation of shrub/grass mixed. The lower right corner (fire scars of 1987 and 1994) shows both positive and negative GPP difference, indicating a complex recovery pattern. The prefire vegetation of this area was primarily evergreen needleleaf forest, but postfire vegetation was primarily deciduous broadleaf forest and shrub/grass mixed. This general qualitative assessment could be further quantitatively analyzed based on the statistics of GPP (Table 2).

Table 2 shows the GPP comparison. The actual mean GPPs for the 0-year 2004 fire scar in July, August, and September are 23, 16, and 5 gC/m²/month, but the reconstructed means are 122, 38, and 26 gC/m²/month, resulting in a negative GPP difference of -99, -22, and -21 gC/m²/month. The recovery ratio is 24%. The 2004 Landsat images were acquired immediately after the 2004 fire event; therefore, the low GPP recovery rate (24%) indicates that the most recent fires significantly damaged the vegetation cover. The 1-year 2003 fire scar shows a similar pattern to the 2004 fire scar, but the recovery rate is 43%, a little higher than the 24% of the 2004 fire scar. This rate indicates that the recovery was still at a low level, but the recovery of the 2003 fire scar was better than that of the 2004 fire scar. The actual mean GPPs for the 17-year 1987 fire scar in July, August, and September are 112, 73, and 21 gC/m²/month, but the reconstructed means are 120, 82, and 25 gC/m²/month, resulting in a negative GPP difference of only -8, -10, and -4 gC/m²/month. The recovery ratio is up to 91%. This rate indicates that the GPP almost recovered to prefire level. In those fire scars from burns in 1991, 1995, 1998, 2001, and 2002,

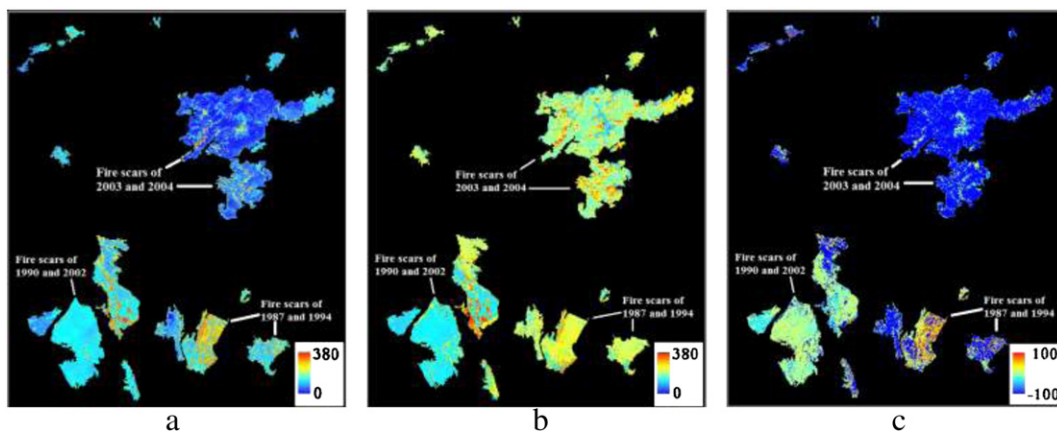


Fig. 6. The impact of fires and succession on GPP (gC/m²). a) Total GPP in July, August, and September 2004, b) total GPP in July, August, and September 2004 assuming fire has not occurred, and c) GPP difference between a and b. Black areas are cloud, shadow, and unburned areas. The images cover the same area as Fig. 1.

Table 2
The comparison of actual postfire and reconstructed GPP ($\text{gC}/\text{m}^2/\text{month}$) for different fire scars.

Burning year (age ^a)	Actual postfire scenario in 2004						Assuming-no-fire scenario						Difference						Ratio (%) ^c			
	Postfire land cover (EF/DF/SG ^b)	July GPP		Aug GPP		Sept GPP		Prefire land cover (EF/DF/SG ^b)	July GPP		Aug GPP		Sept GPP		Land CC (EF/DF/SG ^b)	July GPP		Aug GPP		Sept GPP		
		avg	std	avg	std	avg	std		avg	std	avg	std	avg	std		avg	std	avg		std	avg	std
1987 (17)	4/50/46	112	51	73	33	21	10	74/11/15	120	29	82	21	25	6	-70/39/31	-8	47	-10	28	-4	9	91
1990 (14)	4/7/89	60	30	51	23	13	8	75/6/19	116	30	87	24	26	8	-71/1/70	-55	38	-37	28	-13	10	54
1991 (13)	6/18/76	79	29	61	22	15	6	20/7/73 ^d	114	32	66	28	16	8	-14/11/3	-35	37	-5	23	-2	7	79
1993 (11)	4/8/88	61	28	45	21	11	5	72/5/23	112	31	76	22	23	7	-68/3/65	-51	36	-30	25	-12	7	55
1994 (10)	2/23/75	77	41	50	26	14	8	83/3/14	113	25	73	16	24	6	-81/20/61	-36	43	-24	25	-10	9	67
1995 (9)	8/30/62	92	42	61	27	16	7	47/5/48 ^d	94	33	64	22	19	7	-39/25/14	-2	32	-3	19	-3	6	95
1998 (6)	6/26/68	86	46	60	33	16	9	43/18/39 ^d	109	45	72	30	22	10	-37/8/29	-23	38	-11	23	-7	8	80
1999 (5)	4/12/84	60	35	39	23	12	7	78/5/17	113	28	63	21	24	7	-74/7/67	-54	39	-24	21	-12	8	56
2000 (4)	13/7/80	53	41	53	25	14	7	53/5/42	102	38	73	27	20	9	-40/2/38	-49	46	-20	26	-6	8	62
2001 (3)	2/10/88	75	33	52	23	14	6	45/6/49 ^d	98	39	71	28	20	9	-43/4/39	-23	42	-19	28	-6	9	75
2002 (2)	2/2/96	63	23	45	14	12	5	15/4/81 ^d	79	32	53	21	16	7	-13/-2/15	-16	36	-7	19	-4	8	81
2003 (1)	8/5/87	47	37	34	26	9	8	73/16/11	125	34	58	28	27	9	-65/-11/76	-79	43	-24	20	-18	10	43
2004 (0)	6/3/91	23	35	16	27	5	7	74/12/14	122	34	38	31	26	8	-68/-9/77	-99	47	-22	16	-21	10	24

^a The age of a fire scar is the time difference between 2004 and the burning year.

^b EF/DF/SG refers to the % of evergreen needleleaf forest, deciduous broadleaf forest, and shrub/grass mixed.

^c The ratio is the "actual postfire total GPP from July to September" divided by the "assuming-no-fire total GPP from July to September," which is an indicator of recovery rate.

^d Prefire land covers were dominated by shrub/grass, represented by solid symbols in Fig. 7.

the recovery rates are all greater than 75%. Before the fires, these areas were dominated by shrub/grass (see the land cover in Table 2), indicating shrub/grass might recover faster than evergreen needleleaf forest. The faster recovery rates of shrub/grass can be better observed in Fig. 7, where their values are at high level and all greater than 75%.

The overall assessment based on the mean values in Table 2 helps to understand the general trend as mentioned above; however, the standard deviations within the 1987–2004 fire scars, which were presented in Table 2 for actual and reconstructed GPP as well as their difference, indicate the variability within the same burned area. These standard deviation values imply the spatial heterogeneity, which is related to local site environment and burn severity. Our approach allows for pixel-by-pixel analysis on the impact of fires and succession on GPP and is revealed in Fig. 6c, where isolated patches deviating from the general distribution even within the same fire scars are visible. For example, over 10 patches within the 2004 fire scar show obvious GPP differences compared to their neighboring areas.

To further investigate the spatial variation, a small area was selected for careful examination (Fig. 8). Before the fire in 1998, this area was covered by evergreen needleleaf forest (54%), deciduous broadleaf forest (11%), and shrub/grass mixed (35%) (Fig. 8a). After the fire, their cover percentages changed to 11%, 20%, and 69% for evergreen needleleaf forest, deciduous broadleaf forest, and shrub/grass mixed, respectively (Fig. 8b). Due to this fire disturbance, when we compared the reconstructed GPP (Fig. 8c) with actual postfire GPP (Fig. 8d), the originally forested areas were subject to reduced GPP after 6 years;

however, the originally shrub/grass areas had an increased GPP (Fig. 8e). This phenomenon can be better observed in the recovery ratio (Fig. 8f), where the originally forested areas show a ratio of less than 1, while the originally shrub/grass areas show a ratio of close to or greater than 1.

6. Discussion

Postfire vegetation recovery depends on many factors such as fire scar age, prefire vegetation, burn severity, soil, drainage, weather, and seed availability (Li and Potter, 2012). In our study, we revealed different changes in GPP for those fire scars with different ages (Table 2). Kasischke and French (1997) used 2 years of NDVI after fire and found a 50% reduction. Goetz et al. (2006) found that the burned areas displayed a sharp drop in NDVI at the time of the burning, followed by a recovery to pre-burn levels within about 5 years. Epting and Verbyla (2005) found NDVI values dropped sharply for 2 years following the fire and then increased until reaching a peak in year 14. Hicke et al. (2003) modeled NPP of the most impacted pixel within each burned area and estimated a mean recovery period for boreal forests of about 9 years, with substantial variability among fires. Bond-Lamberty et al. (2004) measured total NPP and found it was low immediately after fire but highest 12–20 years after fire. Goulden et al. (2011) found an increasing trend in average GPP at stands that are 6, 15, and 23 years old. All these NDVI, LAI, NPP, and GPP changes indicate vegetation damage and recovery on the surface. In general, our GPP showed only 24% and 43% for the 0-year (immediate 2004 fire) and 1-year 2003 fire scar, which coincided with previous observations. However, we found that after 2 years the recovery rate ranged from 54% to 95%. Our study confirmed that fire scar age affects GPP recovery, but its influence is not absolute; spatial heterogeneity (e.g., prefire vegetation type) also played an important role as demonstrated in Fig. 8, where notable spatial variation of GPP recovery even within the same fire scar is obvious.

The approach we demonstrated in this study can quantify fire-induced GPP change at the pixel level. Satellite vegetation index has been used to estimate postfire vegetation recovery (e.g., Kasischke and French, 1997; Epting and Verbyla, 2005; Goetz et al., 2006; Cuevas-Gonzalez et al., 2009; Veraverbeke et al., 2012). We further used NDVI as an input for a light-use efficiency GPP model so that the magnitude change in primary productivity caused by fire disturbance (i.e., the change in carbon fixation by vegetation) can be modeled. In this model, the changes in E_{max} and F_{PAR} are critical information. Successional trajectory varies in interior Alaska, resulting in a different

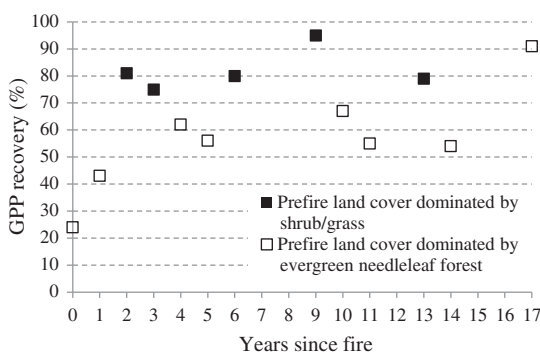


Fig. 7. Percent recovery of GPP following fire disturbance stratified by prefire vegetation type.

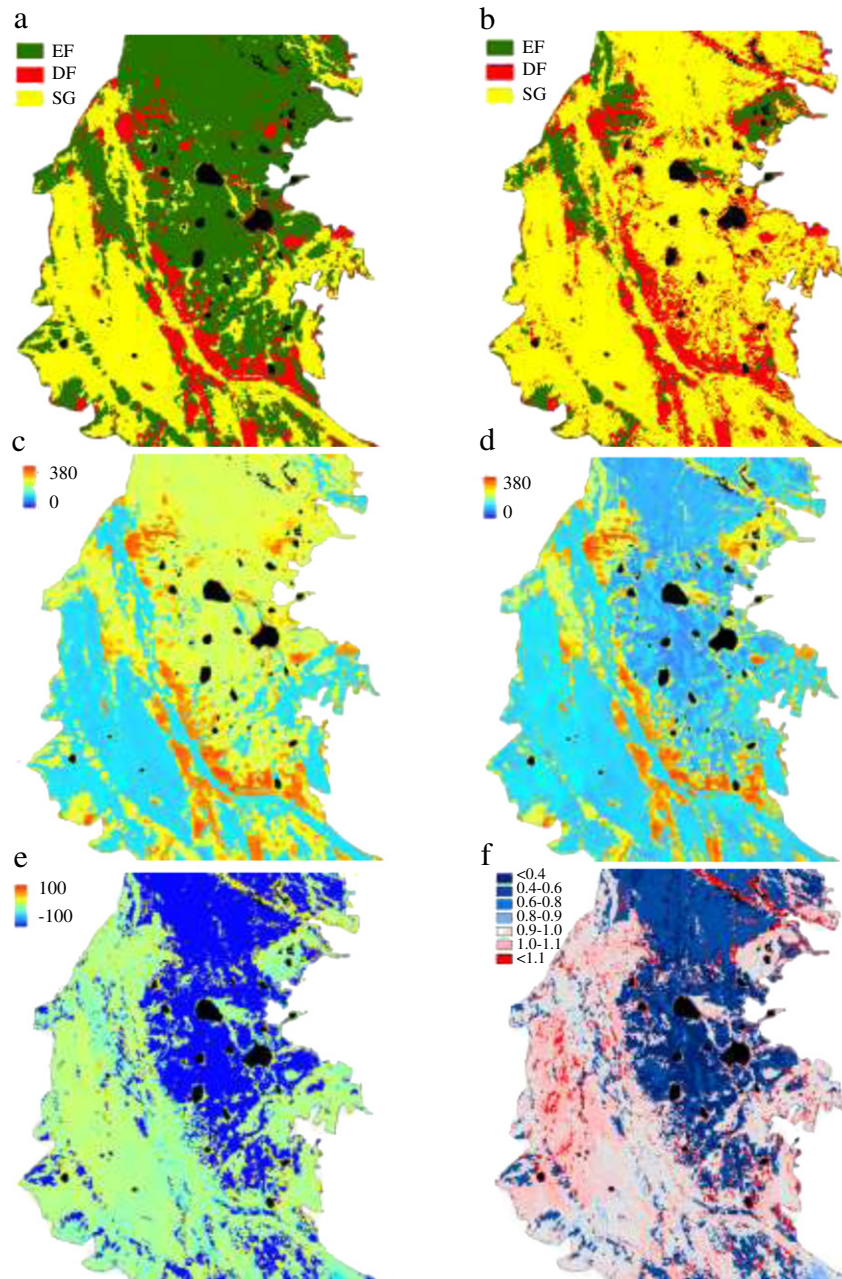


Fig. 8. A selected area (see white box in Fig. 1) burned in 1998. The black areas are water bodies. a) Prefire (1986) Landsat classification, b) postfire (2004) classification, c) total GPP in July, August, and September 2004 assuming no fires had occurred (gC/m^2), d) total GPP in July, August, and September 2004 (gC/m^2), e) difference between actual and reconstructed GPP (i.e., d–c), f) ratio of actual to reconstructed GPP (i.e., d/c). In a and b, EF is evergreen needleleaf forest, DF is deciduous broadleaf forest, and SG is shrub/grass mixed. Width 10.5 km and height 11.5 km.

vegetation type after fire disturbance (Beck et al., 2011; Johnstone et al., 2010). The E_{max} value for different vegetation types can be modeled from the eddy covariance technique, which was demonstrated in our 1987 burn, 1999 burn, and unburned control flux tower sites. After fire, the canopy structure changed, resulting in the F_{PAR} change, which was inferred from NDVI change based on the local relationship found by Steinberg et al. (2006). Based on the spatially explicit change in E_{max} and F_{PAR} , the spatial variation of fire impact on GPP, which is caused by site-specific environment and climate variability, can be captured. This was achieved by reconstructing satellite images assuming the fires had not occurred, with details reported in Huang et al. (2013). Our products advanced the work of Randerson et al. (2006), who used a single fire to quantify the various forcing agents, including ecosystem production, and their combined effect on climate warming.

Single fire study is a necessary step toward assessing the impact of a changing boreal fire regime on climate at regional or continental scales, and our spatially explicit GPP change quantification at the pixel level further advanced the estimation of fire effect on climate change. However, there are some limitations in our work as follows.

First, F_{PAR} estimation could be biased by non-photosynthetic vegetation (NPV). Vegetation canopies are composed of chlorophyll and NPV, but only the PAR absorbed by chlorophyll is responsible for photosynthesis; therefore, ideally canopy-level F_{PAR} should be partitioned into the fraction of PAR absorbed by chlorophyll and by NPV (Xiao, 2006). This may be more important for a fire-disturbed ecosystem because a large portion of coarse woody debris will remain after fire events (Huang et al., 2009; Liu et al., 2011). In this study, we did not consider the NPV effect.

Table 3
The E_{\max} (in unit of gC/mol PAR) comparison between our study and previous studies.

Sites	This study ^a	Other studies	Reference/notes
Evergreen needleleaf forest (Control)	0.2508	0.24	Ruimy et al. (1996)
		0.14	Prince and Goward (1995)
		0.22	Running et al. (2000)
		0.48	Law et al. (2000) and Xiao et al. (2005)
		0.48 ^b	Goulden et al. (1997)
Deciduous broadleaf forest (1987 burn)	0.2904	0.49 ^b	Sullivan et al. (1997)
		0.24	Ruimy et al. (1996)
		0.146	Prince and Goward (1995)
		0.227	Running et al. (2000)
Shrub/grass mixed (1999 burn)	0.1104	0.528	Xiao et al. (2004b) and Wofsy et al. (1993)
		0.018 ^b	Li et al. (2007) (for shrub)
		0.020 ^b	Li et al. (2007) (for meadow)
		0.30 ^b	Ruimy et al. (1996) (for grassland)
		0.37	Wang et al. (2010b) (for degraded grassland)

^a Data from Table 1.

^b The original unit is in $\mu\text{mol CO}_2/\mu\text{mol PPF}$, but here converted to gC/mol PAR using a scalar of 12.001.

Second, the three E_{\max} values determined in our study may not be sufficient. The E_{\max} is an important parameter that heavily relies on vegetation types but can be estimated from continuous CO_2 eddy flux towers (Wofsy et al., 1993). In our study, we used three flux towers to estimate E_{\max} for the local three representative ecosystems associated with fire disturbance. Although our estimations are between the previously reported E_{\max} (Table 3), land use change, disturbance history, and different successional stages of vegetation may result in the spatial variation and temporal changes of E_{\max} within a biome type (Wang et al., 2010a; Xiao, 2006), and a biome-dependent E_{\max} might be inappropriate due to the large inter-site difference (Wang and Zhou, 2012). This problem may be enhanced by the heterogeneity of a pixel, where different vegetation types may coexist and discrete land cover classification might not distinguish the real world vegetation types (Lavoie and Mack, 2012; Wang et al., 2010a). The problem may be also influenced by the quality of the flux measurements themselves. NEE measurements are affected by instrument calibration and data quality control. Perhaps a larger source of uncertainty comes from partitioning NEE into GPP and Re for E_{\max} calculation by extrapolating the relationship between nighttime respiration and soil temperature to daytime respiration. Both NEE and respiration decisions are subjective, and are currently subject to great discussion (Wang et al., 2010a).

Third, the GPP change revealed in the current study only reflects the conditions of three Landsat acquisitions in 2004 due to the 16-day repeat frequency and cloud cover. The hottest summer in at least the past 200 years occurred in 2004 (Barber et al., 2004) and the drought resulted in low vegetation production and different drought response sensitivity between aspen and black spruce (Welp et al., 2007). The approach demonstrated in this study using limited images in a limited extent shows promising results for extrapolating site-specific field or flux observations to a regional area; however, a fuller analysis of interannual and seasonal dynamics is desired. Extending this analysis to more Landsat overpasses would be able to address the interannual and seasonal dynamics.

7. Summary and conclusion

Boreal wildfires and succession change the land surface, including vegetation type and coverage, and carbon fixation. Due to the importance of fires in the carbon cycle and climate change, it is critical to quantify the effect of fire and succession on the dynamics of GPP. Point-based observations such as eddy covariance help us understand the carbon uptake, but its weakness of spatial representation hampers an analysis over a large area. Satellite-derived data such as NDVI or LAI can provide spatial-temporal vegetation information, but direct vegetation index comparison cannot reveal GPP magnitude. The direct prefire and postfire comparison is widely used, but the recovery identification may become

biased due to interannual climate variability. Our approach used an image reconstruction that minimizes the confounding factors of weather variability, seasonal offset, topography, land cover, and drainage. This reconstruction reveals spatially explicit change in NDVI and F_{PAR} between the actual postfire and assuming-no-fire scenarios (Huang et al., 2013). The information can be incorporated into a light-use efficiency model for estimating GPP. This model requires an important parameter E_{\max} that differs for different vegetation type, which can also be changed by fires and succession. The E_{\max} can be derived from eddy covariance data. By integrating the changes in E_{\max} and F_{PAR} into the light-use efficiency model, the spatially explicit GPP change and recovery caused by fires could be examined. A future study will apply the approach demonstrated here to multitemporal fire impact on GPP over a large area.

Acknowledgments

This work was supported by the U.S. Geological Survey Climate and Land Use, Research and Development, and Climate Effect Network programs. The authors greatly thank Dr. James Randerson at University of California for providing the flux tower data, Dr. Stephanie McAfee for climate data, Dr. Shuang Li for internally reviewing the manuscript, and Thomas Adamson and Sandra Cooper for revising the English. Any use of trade, product, or firm names is for descriptive purposes only and does not imply endorsement by the U.S. Government.

References

- Amiro, B. D., Barr, A. G., Barr, J. G., Black, T. A., Bracho, R., Brown, M., et al. (2010). Ecosystem carbon dioxide fluxes after disturbance in forests of North America. *Journal of Geophysical Research*, 115, G00K02. <http://dx.doi.org/10.1029/2010JG001390>.
- Amiro, B. D., Chen, J. M., & Liu, J. (2000). Net primary productivity following forest fire for Canadian ecoregions. *Canadian Journal of Forest Research*, 30(6), 939–947.
- Baldocchi, D., Falge, E., Gu, L., Olson, R., Hollinger, D., Running, S., et al. (2001). FLUXNET: A new tool to study the temporal and spatial variability of ecosystem-scale carbon dioxide, water vapor, and energy flux densities. *Bulletin of the American Meteorological Society*, 82, 2415–2434.
- Barber, V. A., Juday, G. P., Finney, B. P., & Wilmking, M. (2004). Reconstruction of summer temperatures in interior Alaska from tree-ring proxies: Evidence for changing synoptic climate regimes. *Climatic Change*, 63, 91–120.
- Beck, P. S. A., & Goetz, S. J. (2011). Satellite observations of high northern latitude vegetation productivity changes between 1982 and 2008: Ecological variability and regional differences. *Environmental Research Letters*, 6, 045501. <http://dx.doi.org/10.1088/1748-9326/6/4/045501>.
- Beck, P. S. A., Goetz, S. J., Mack, M. C., Alexander, H. D., Jin, Y., Randerson, J. T., et al. (2011). The impacts and implications of an intensifying fire regime on Alaskan boreal forest composition and albedo. *Global Change Biology*, 17(9), 2853–2866. <http://dx.doi.org/10.1111/j.1365-2486.2011.02412.x>.
- Bond-Lamberty, B. C., Peckham, S. D., Ahl, D. E., & Gower, S. T. (2007). Fire as the dominant driver of central Canadian boreal forest carbon balance. *Nature*, 450(7166), 89–92. <http://dx.doi.org/10.1038/nature06272>.
- Bond-Lamberty, B., Wang, C., & Gower, S. T. (2004). Net primary production and net ecosystem production of a boreal black spruce fire chronosequence. *Global Change Biology*, 10(4), 473–487. <http://dx.doi.org/10.1111/j.1529-8817.2003.0742.x>.

- Cuevas-González, M., Gerard, F., Balzter, H., & Riaño, D. (2009). Analysing forest recovery after wildfire disturbance in boreal Siberia using remotely sensed vegetation indices. *Global Change Biology*, 15, 561–577. <http://dx.doi.org/10.1111/j.1365-2486.2008.01784.x>.
- Epting, J., & Verbyla, D. (2005). Landscape-level interactions of prefire vegetation, burn severity, and postfire vegetation over a 16-year period in interior Alaska. *Canadian Journal of Forest Research*, 35(6), 1367–1377.
- Field, C. B., Randerson, J. T., & Malmstrom, C. M. (1995). Global net primary production—Combining ecology and remote-sensing. *Remote Sensing of Environment*, 51, 74–88.
- Frolking, S. E., Bubier, J. L., Moore, T. R., Ball, T., Bellisario, L. M., Bhardwaj, A., et al. (1998). Relationship between ecosystem productivity and photosynthetically active radiation for northern peatlands. *Global Biogeochemical Cycles*, 12, 115–126.
- Goetz, S. J., Bond-Lamberty, B., Law, B. E., Hicke, J. A., Huang, C., Houghton, R. A., et al. (2012). Observations and assessment of forest carbon dynamics following disturbance in North America. *Journal of Geophysical Research*, 117(G02022). <http://dx.doi.org/10.1029/2011JG001733>.
- Goetz, S. J., Gregory, J. F., & Andrew, G. B. (2006). Using satellite time-series data sets to analyze fire disturbance and forest recovery across Canada. *Remote Sensing of Environment*, 101(3), 352–365.
- Goetz, S. J., Prince, S. D., Goward, S. N., Thawley, M. M., & Small, J. (1999). Satellite remote sensing of primary production: An improved production efficiency modeling approach. *Ecological Modelling*, 122(3), 239–255.
- Goulden, M. L., Daube, B. C., Fan, S. M., Sutton, D. J., Bazzaz, A., Munger, J. W., et al. (1997). Physiological responses of a black spruce forest to weather. *Journal of Geophysical Research-Atmospheres*, 102, 28987–28996.
- Goulden, M. L., McMillan, A., Winston, G. C., Rocha, A. V., Manies, K. L., Harden, J. W., et al. (2011). Patterns of NPP, GPP, respiration and NEP during boreal forest succession. *Global Change Biology*, 17(2), 855–871. <http://dx.doi.org/10.1111/j.1365-2486.2010.02274.x>.
- Goulden, M. L., Winston, G. C., McMillan, A., Litvak, M., Read, E. L., Rocha, A. V., et al. (2006). An eddy covariance mesonet to measure the effect of forest age on land-atmosphere exchange. *Global Change Biology*, 12, 2146–2162. <http://dx.doi.org/10.1111/j.1365-2486.2006.01251.x>.
- Hicke, J. A., Asner, G. P., Kasischke, E. S., French, N. H. F., Randerson, J. T., Collatz, G. J., et al. (2003). Postfire response of North American boreal forest net primary productivity analyzed with satellite observations. *Global Change Biology*, 9(8), 1145–1157.
- Huang, S., Crabtree, R. L., Potter, C., & Gross, P. (2009). Estimating the quantity and quality of coarse woody debris in Yellowstone post-fire forest ecosystem from fusion of SAR and optical data. *Remote Sensing of Environment*, 113(9), 1926–1938.
- Huang, S., Jin, S., Dahal, D., Chen, X., Young, C., Liu, H., et al. (2013). Reconstructing satellite images to quantify spatially explicit land surface change caused by fires and succession: A demonstration in the Yukon River Basin of interior Alaska. *ISPRS Journal of Photogrammetry and Remote Sensing*, 79, 94–105.
- Huang, S., Rich, P., Crabtree, R., Potter, C., & Fu, P. (2008). Modelling near-surface air temperature from solar radiation and lapse rate: Application over complex terrain in Yellowstone National Park, USA. *Physical Geography*, 29(2), 158–178.
- Jin, S., Homer, C., Yang, L., Xian, G., Fry, J., Danielson, P., et al. (2012). Automated cloud and shadow detection and filling using two-date Landsat imagery in the USA. *International Journal of Remote Sensing*, 34(5), 1540–1560.
- Johnstone, J. F., Hollingsworth, T. N., Chapin, F. S., & Mack, M. C. (2010). Changes in fire regime break the legacy lock on successional trajectories in Alaskan boreal forest. *Global Change Biology*, 16(4), 1281–1295. <http://dx.doi.org/10.1111/j.1365-2486.2009.02051.x>.
- Kasischke, E. S., & French, N. H. F. (1997). Constraints on using AVHRR composite index imagery to study patterns of vegetation cover in boreal forests. *International Journal of Remote Sensing*, 18(11), 2403–2426.
- Kasischke, E. S., Loboda, T., Giglio, L., French, N. H. F., Hoy, E. E., de Jong, B., et al. (2011). Quantifying burned area for North American forests: Implications for direct reduction of carbon stocks. *Journal of Geophysical Research*, 116, G04003. <http://dx.doi.org/10.1029/2011JG001707>.
- Kasischke, E. S., & Turetsky, M. R. (2006). Recent changes in the fire regime across the North American boreal region—Spatial and temporal patterns of burning across Canada and Alaska. *Geophysical Research Letters*, 33, L09703. <http://dx.doi.org/10.1029/2006GL025677>.
- Landsberg, J. J., & Waring, R. H. (1997). A generalized model of forest productivity using simplified concepts of radiation use efficiency, carbon balance and partitioning. *Forest Ecology and Management*, 95, 209–228.
- Lavoie, M., & Mack, M. C. (2012). Spatial heterogeneity of understory vegetation and soil in an Alaskan upland boreal forest fire chronosequence. *Biogeochemistry*, 107, 227–239.
- Law, B. E., Waring, R. H., Anthoni, P. M., & Aber, J. D. (2000). Measurements of gross and net ecosystem productivity and water vapour exchange of a *Pinus ponderosa* ecosystem, and an evaluation of two generalized models. *Global Change Biology*, 6, 155–168.
- Li, S., & Potter, C. (2012). Vegetation regrowth trends in post forest fire ecosystems across North America from 2000 to 2010. *Natural Science*, 4(10), 755–770. <http://dx.doi.org/10.4236/ns.2012.41010>.
- Li, Z., Yu, G., Xiao, X., Li, Y., Zhao, X., Ren, C., et al. (2007). Modeling gross primary production of alpine ecosystems in the Tibetan Plateau using MODIS images and climate data. *Remote Sensing of Environment*, 107(3), 510–519.
- Litvak, M., Miller, S., Wofsy, S. C., & Goulden, M. (2003). Effect of stand age on whole ecosystem CO₂ exchange in the Canadian boreal forest. *Journal of Geophysical Research*, 108(D3), 8225. <http://dx.doi.org/10.1029/2001JD000854>.
- Liu, S., Bond-Lamberty, B., Hicke, J. A., Vargas, R., Zhao, S., Chen, J., et al. (2011). Simulating the impacts of disturbances on forest carbon cycling in North America: Processes, data, models, and challenges. *Journal of Geophysical Research, Biogeosciences*, 116, G00K08. <http://dx.doi.org/10.1029/2010JG001585>.
- Liu, H. P., & Randerson, J. T. (2008). Interannual variability of surface energy exchange depends on stand age in a boreal forest fire chronosequence. *Journal of Geophysical Research*, 113, G01006. <http://dx.doi.org/10.1029/2007JG000483>.
- Liu, H. P., Randerson, J. T., Lindfors, J., & Chapin, F. S., III (2005). Changes in the surface energy budget after fire in boreal ecosystems of Interior Alaska: An annual perspective. *Journal of Geophysical Research, Atmosphere*, 110, D13101. <http://dx.doi.org/10.1029/2004JD005158>.
- Lloyd, J., & Taylor, J. A. (1994). On the temperature-dependence of soil respiration. *Functional Ecology*, 8(3), 315–323.
- Lu, J., Sun, G., McNulty, S. G., & Amatya, D. M. (2005). A comparison of six potential evapotranspiration methods for regional use in the southeastern United States. *Journal of the American Water Resources Association*, 41, 621–633.
- Mäkelä, A., Pulkkinen, M. A., Kolari, P., Largergren, F., Berbigier, P., Lindroth, A., et al. (2008). Developing an empirical model of stand GPP with the LUE approach: Analysis of eddy covariance data at five contrasting conifer sites in Europe. *Global Change Biology*, 14, 92–108.
- Maselli, F., Papale, D., Puletti, N., Chirici, G., & Corona, P. (2009). Combining remote sensing and ancillary data to monitor the gross productivity of water-limited forest ecosystems. *Remote Sensing of Environment*, 113, 657–667.
- Mather, P. M. (1987). *Computer processing of remotely-sensed images* (1st ed.). New York: John Wiley & Sons, 287–289.
- McCree, K. J. (1972). Test of current definitions of photosynthetically active radiation against leaf photosynthesis data. *Agricultural Meteorology*, 10, 443–453. [http://dx.doi.org/10.1016/0002-1571\(72\)90045-3](http://dx.doi.org/10.1016/0002-1571(72)90045-3).
- McCree, K. J. (1981). Photosynthetically active radiation. In O. L. Lange, P. S. Nobel, C. B. Osmond, & H. Ziegler (Eds.), *Encyclopedia of plant physiology. New Series, vol. 12-A* (pp. 41–55). Berlin: Springer-Verlag.
- Melillo, J. M., McGuire, A. D., Kicklighter, D. W., Moore, B., Vorosmarty, C. J., & Schloss, A. L. (1993). Global climate-change and terrestrial net primary production. *Nature*, 363, 234–240.
- Potter, C. S., Randerson, J. T., Field, C. B., Matson, P. A., Vitousek, P. M., Mooney, H. A., et al. (1993). Terrestrial ecosystem production—A process model-based on global satellite and surface data. *Global Biogeochemical Cycles*, 7, 811–841.
- Prince, S. D., & Goward, S. N. (1995). Global primary production: A remote sensing approach. *Journal of Biogeography*, 22, 815–835.
- Randerson, J. T., Liu, H. P., Flanner, M. G., Chambers, S. D., Jin, Y., Hess, P. G., et al. (2006). The impact of boreal forest fire on climate warming. *Science*, 341(5802), 1130–1132.
- Reichstein, M., Falge, E., Baldocchi, D., Papale, D., Aubinet, M., Berbigier, P., et al. (2005). On the separation of net ecosystem exchange into assimilation and ecosystem respiration: Review and improved algorithm. *Global Change Biology*, 11, 1424–1439.
- Rind, D., Goldberg, R., Hansen, J., Rosenzweig, C., & Ruedy, R. (1990). Potential evapotranspiration and the likelihood of future drought. *Journal of Geophysical Research*, 95, 9983–10004. <http://dx.doi.org/10.1029/JD095iD07p09983>.
- Ruimy, A., Dedieu, G., & Saugier, B. (1996). TURC: A diagnostic model of continental gross primary productivity and net primary productivity. *Global Biogeochemical Cycles*, 10, 269–285.
- Running, S. W., Thornton, P. E., Nemani, R., & Glassy, J. M. (2000). Global terrestrial gross and net primary productivity from the earth observing system. In O. E. Sala, R. B. Jackson, H. A. Mooney, & R. W. Howarth (Eds.), *Methods in ecosystem science* (pp. 44–57). New York: Springer.
- Schulze, E. D., Lloyd, J., Kelliher, F. M., Wirth, C., Rebmann, C., Luhker, B., et al. (1999). Productivity of forests in the Eurosiberian boreal region and their potential to act as a carbon sink—A synthesis. *Global Change Biology*, 5, 703–722.
- Shenoy, A., Johnstone, J. F., & Kasischke, E. S. (2011). Persistent effects of fire severity on early successional forests in interior Alaska. *Forest Ecology and Management*, 261(3), 381–390.
- Steinberg, D. C., Goetz, S. J., & Hyer, E. J. (2006). Validation of MODIS F_{PAR} products in boreal forests of Alaska. *IEEE Transactions on Geoscience and Remote Sensing*, 44(7), 1818–1828. <http://dx.doi.org/10.1109/TGRS.2005.862266>.
- Sullivan, J. H., Bovard, B. D., & Middleton, E. M. (1997). Variability in leaf-level CO₂ and water fluxes in *Pinus banksiana* and *Picea mariana* in Saskatchewan. *Tree Physiology*, 17, 553–561.
- Tucker, C. J. (1979). Red and photographic infrared linear combinations for monitoring vegetation. *Remote Sensing of Environment*, 8, 127–150.
- Ueyama, M., Harazono, Y., & Ichii, K. (2010). Satellite-based modeling of the carbon fluxes in mature black spruce forests in Alaska: A synthesis of the eddy covariance data and satellite remote sensing data. *Earth Interactions*, 14(13), 1–27. <http://dx.doi.org/10.1175/2010EI319.1>.
- Veraverbeke, S., Gitas, I., Katagis, T., Polychronaki, A., Somers, B., & Goossens, R. (2012). Assessing post-fire vegetation recovery using red–near infrared vegetation indices: Accounting for background and vegetation variability. *ISPRS Journal of Photogrammetry and Remote Sensing*, 68, 28–39.
- Wang, H., Jia, G., Fu, C., Feng, J., Zhao, T., & Ma, Z. (2010a). Deriving maximal light use efficiency from coordinated flux measurements and satellite data for regional gross primary production modeling. *Remote Sensing of Environment*, 114(10), 2248–2258.
- Wang, Z., Xiao, X., & Yan, X. (2010b). Modeling gross primary production of maize cropland and degraded grassland in northeastern China. *Agricultural and Forest Meteorology*, 150, 1160–1167.
- Wang, Y., & Zhou, G. (2012). Light use efficiency over two temperate steppes in inner Mongolia, China. *PLoS One*, 7(8), e43614. <http://dx.doi.org/10.1371/journal.pone.0043614>.
- Welp, L. R., Randerson, J. T., & Liu, H. P. (2006). The influence of stand age on seasonal exchange of CO₂ and d¹⁸O-CO₂ from a boreal forest fire chronosequence. *Journal of Geophysical Research*, 111, G03007. <http://dx.doi.org/10.1029/2005JG000126>.

- Welp, L. R., Randerson, J. T., & Liu, H. P. (2007). The sensitivity of carbon fluxes to spring warming and summer drought depends on plant functional type in boreal forest ecosystems. *Agricultural and Forest Meteorology*, *147*, 172–185. <http://dx.doi.org/10.1016/j.agrformet.2007.07.010>.
- Wofsy, S. C., Goulden, M. L., Munger, J. W., Fan, S. M., Bakwin, P. S., Daube, B. C., et al. (1993). Net exchange of CO₂ in a mid-latitude forest. *Science*, *260*, 1314–1317.
- Xiao, X. (2006). Light absorption by leaf chlorophyll and maximum light use efficiency. *IEEE Transactions on Geoscience and Remote Sensing*, *44*(7), 1933–1935.
- Xiao, J., Chen, J., Davis, K. J., & Reichstein, M. (2012). Advances in upscaling of eddy covariance measurements of carbon and water fluxes. *Journal of Geophysical Research*, *117*, G00J01. <http://dx.doi.org/10.1029/2011JG001889>.
- Xiao, X., Hollinger, D., Aber, J. D., Goltz, M., Davidson, E. A., & Zhang, Q. Y. (2004a). Satellite-based modeling of gross primary production in an evergreen needleleaf forest. *Remote Sensing of Environment*, *89*, 519–534.
- Xiao, X. M., Zhang, Q., Braswell, B., Urbanski, S., Boles, S., Wofsy, S. C., et al. (2004b). Modeling gross primary production of temperate deciduous broadleaf forest using satellite images and climate data. *Remote Sensing of Environment*, *91*, 256–270.
- Xiao, X. M., Zhang, Q. Y., Hollinger, D., Aber, J., & Moore, B. (2005). Modeling gross primary production of an evergreen needleleaf forest using MODIS and climate data. *Ecological Applications*, *15*(3), 954–969. <http://dx.doi.org/10.1890/04-0470>.
- Xiao, J., Zhuang, Q., Law, B. E., Chen, J., Baldocchi, D. D., Cool, D. R., et al. (2010). A continuous measure of gross primary production for the conterminous United States derived from MODIS and AmeriFlux data. *Remote Sensing of Environment*, *114*(3), 576–591.
- Yi, S., McGuire, A. D., Kasischke, E., Harden, J., Manies, K., Mack, M., et al. (2010). A dynamic organic soil biogeochemical model for simulating the effects of wildfire on soil environmental conditions and carbon dynamics of black spruce forests. *Journal of Geophysical Research*, *115*, G04015. <http://dx.doi.org/10.1029/2010JG001302>.
- Zha, T., Kellomaki, S., Wang, K. Y., & Rouvinen, I. (2004). Carbon sequestration and ecosystem respiration for 4 years in a Scots pine forest. *Global Change Biology*, *10*, 1492–1503.